Construction and Building Materials 412 (2024) 134889

Contents lists available at ScienceDirect

Construction and Building Materials

journal homepage: www.elsevier.com/locate/conbuildmat

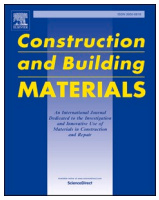

Low permeability sealing materials based on sewage, digestate and incineration industrial by-products in the final landfill cover system

Xuan Ling [a,b,*], Wei Chen [a], Katrin Schollbach [b], H.J.H. Brouwers [a,b]

[a] State Key Laboratory of Silicate Materials for Architectures, Wuhan University of Technology, Wuhan 430070, China
[b] Department of the Built Environment, Eindhoven University of Technology, P.O. Box 513, 5600 MB Eindhoven, the Netherlands

ARTICLE INFO

Keywords:
Sewage sludge
Sealing material
Permeability
Gel characterization

ABSTRACT

This study explores repurposing municipal solid waste from the sewage, digestate, and incineration industries as landfill-sealing materials, aligning with circular economy principles. The main materials include digested sewage sludge (DSS), pretreated digested sewage sludge (PDSS), and digestate sludge (DS), with biomass bottom ash (BBA) and Al-anodizing waste (AAW) introduced as additives, complemented by 1.5 wt% water glass to enhance the sealing performance. The research evaluates the characteristics of the various treated and sourced sludges and additives, assessing their influence on water permeability, reaction products and the environmental consequences. Results demonstrate the achievement of low permeability in the sludge-based sealing materials, with optimal performance observed in the specimens prepared with DSS and AAW (k value = 3.78 $\times 10^{-12}$ m/s). Thermal Pressure Hydrolysis pre-treatment in sewage plants reduces the organic content in PDSS, resulting in a slight increase in permeability. DS-based specimens exhibit higher permeability due to their relatively lower organic content in DS. Gypsum is the primary reaction product attributed to leachable sulphate in BBA and AAW. Water glass addition in BBA-modified specimens promotes silica gel formation, while AAW effectively reduces matrix permeability as an externally added gel-like substance. Additionally, heavy metals (As, Pb and Cr) derived from the by-products are effectively immobilized in the sealing materials owning to the coagulation effect of organic matter in the sludge and sulphates in the products. Overall, this novel approach to landfill sealing materials exhibits promising applications in the Netherlands, offering cost savings and reduced environmental impact by recycling industrial by-products.

1. Introduction

Sewage sludge is the residual solid waste after sewage treatment in wastewater treatment plants (WWTPs). It primarily consists of organic and inorganic compounds separated from the liquid influent through various treatment processes (i.e. primary and secondary). Additional treatments such as anaerobic digestion, aerobic digestion, dewatering and drying are often conducted to reduce the sludge volume and stabilize its composition [1]. In the past, sewage sludge was mostly applied to agricultural soils as fertilizer due to its highly valuable nutrients (N, P and K) [2]. However, stricter regulations (EU Sludge Directive 86/278/EC) have been implemented in EU countries to prevent the uptake of pathogens and heavy metals by crops [3], which results in a significant shift in sludge disposal practices. In the Netherlands, sewage sludge production (dry solid) exceeded 300 thousand tons in 2020, with nearly 85% of the sewage sludge being incinerated [4]. While incineration significantly reduces volume and breaks down organic pollutants, it raises concerns regarding higher emissions of pollutants (nitrogen oxides, sulfur dioxide) and ash disposal costs. Consequently, finding environmentally friendly and cost-effective approaches for sludge treatment and resource utilization has emerged as a crucial scientific and technological challenge [5].

A landfill cover is a protective barrier placed over a landfill site to control landfill gas escape and minimize rainwater infiltration into the waste. It typically consists of multiple layers of materials carefully engineered to serve various functions (Fig. 1). Currently, compacted clay (clay-contained) materials and high-density polyethene (HDPE) geomembrane are often used as the sealing layer materials in a landfill cover system, attributed to their low permeability and high unconfined compressive strength [6,7]. However, traditional compacted clay covers may experience shrinking or swelling under different humidity conditions, leading to cracks and deformations. Therefore, developing new

* Corresponding author at: State Key Laboratory of Silicate Materials for Architectures, Wuhan University of Technology, Wuhan 430070, China.
E-mail address: X.ling@tue.nl (X. Ling).

https://doi.org/10.1016/j.conbuildmat.2024.134889
Received 26 July 2023; Received in revised form 20 December 2023; Accepted 2 January 2024
Available online 6 January 2024

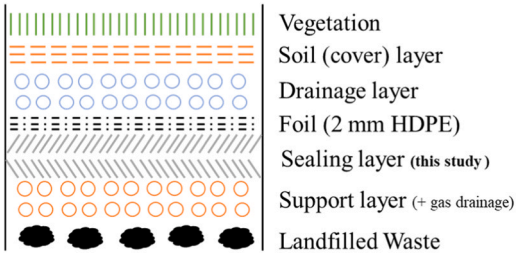

Fig. 1. Schematic of the layer structure in a final landfill cover system. (modified from [14]).

materials for landfill sealing has recently garnered widespread attention [8–13].

Utilizing sewage sludge to formulate a sealing barrier for landfill covers is an effective and ecological recycling strategy that aligns with the objectives of the European Green Deal to promote circularity in resource management and recovery [15]. Li et al. employed fly ash, lime and ferric chloride to dehydrate sludge, and the dewatered sludge was fabricated into a landfill covering material with a permeability coefficient from 10^{-10} to 10^{-7} m·s^{-1} [16]. Oh and Shin prepared the solidified/stabilized dye sludge char with lime, ladle slag and hydroxyapatite and revealed the applicability as a landfill cover material through hydraulic conductivity and micro-structural analysis [17]. Rosli et al. proposed recycling sewage sludge and red gypsum as potential materials for temporary landfill covers. They found an optimum compressive strength of 524 kPa was achieved when the ratio of sewage sludge to red gypsum was 1:1 [18]. Kim et al. used converter slag and lime to solidify digested sewage sludge, and the solidified sludge exhibited desirable geotechnical properties as landfill cover [19]. Liu et al. used industrial calcium-containing waste, including slag, desulfurized gypsum and fly ash, to modify the municipal dewatered sludge, and the hydraulic conductivity of the modified sludge was characterized after six wet-dry cycles to ensure its long-term stability during the local rainy season [20]. The studies mentioned above have explored the modifications of sewage sludge into landfill cover material using various additives. The results showed that sewage sludge exhibited promising impermeability, and the formation of calcium silicate hydrate (C-S-H: $CaO{\cdot}SiO_2{\cdot}nH_2O$) played an important role in the binding and stabilization of the sludge [17–20]. However, most research has focused on various modifications of sewage sludge, disregarding the impact of sludge properties on sealing performance. Given the increasing need to recycle sludge from diverse industrial processes and wastewater treatment systems, it is crucial to investigate the application of different sludge qualities. Notably, the physicochemical properties of sewage sludge are influenced by the treatment process and the effluent source, which is further influenced by regional technological developments and management practices associated with the sludge. In the Netherlands, the main types of sewage sludge generated include normally digested sewage sludge (DSS), digested sewage sludge pretreated (PDSS) with a Thermal Pressure Hydrolysis (TPH) process to enhance biogas production and dewaterability [21,22], and digestate sludge (DS) derived from the organic municipal waste. This research aims to contribute to the energy-efficient disposal of various sludges while providing fundamental theoretical support for regulating their applications.

In sealing materials, achieving low permeability is crucial as it effectively restricts the flow of liquids or gases through the materials. Current strategies for enhanced sealing performance primarily focus on optimizing the physical compaction of the matrix and utilizing chemical reaction products to fill the voids [23]. Wiśniewska and Stępniewski proposed using quick lime and water glass to effectively reduce the permeability of waste rock from coal mining [24]. The C-S-H gel forms in the void space, reducing porosity and binding the grains. However, to minimize the reliance on lime as an additive and explore more sustainable alternatives, the present study adopts a lime-containing industrial by-product, namely biomass bottom ash, derived from the biomass grate furnace. This approach minimizes environmental impact while still achieving the desired sealing performance.

While there has been extensive research on the in-situ generation of C-S-H gel in sludge-based sealing materials, the impact of externally added gel (amorphous) materials is often overlooked due to the associated increase in cost. However, a viable alternative approach is to explore the utilization of industrial solid waste materials that possess similar properties, thereby alleviating cost concerns. One such material is Al-anodizing waste (AAW), a by-product generated during aluminium anodizing. AAW predominantly comprises various $Al(OH)_3$ polymorphs, with approximately 80% of its structure being amorphous [25]. It is noteworthy that EU countries produce an estimated annual quantity of 100,000 metric tonnes of AAW [26]. In this study, we proposed the application of AAW in sludge-based sealing materials, aiming to harness its unique characteristics, such as its amorphous structure and ultra-fine particle size.

To the best of our knowledge, few studies have explored the impact of BBA and AAW in preparing sludge-based sealing materials. Therefore, this investigation aims to establish an effective system for recycling and reusing the above industrial waste by focusing on the sealing performance of various sludge-based materials, the influence of BBA on gel formation, and the feasibility of utilizing AAW as an external gel to enhance sealing performance. Industrial by-products from local plants in the Netherlands are characterized and used to develop environmentally friendly sealing materials that could be used in a final landfill cover system. Comprehensive laboratory-scale analyses are conducted to assess geotechnical properties, reaction processes, microstructure, water permeability and leaching behavior. The findings in this research contributes to sustainable waste management and resource utilization.

2. Materials and experiments

2.1. Materials

The present work assesses the feasibility of using three types of sludge as sealing materials for landfill covers. The sludge types include Digested sewage sludge (DSS) and Pretreated digested sewage sludge (PDSS) obtained from Waste Water Treatment Plants (WWTPs) (Deventer, Netherlands), where the activated sludge with biological chemical phosphate and nitrogen removal process is applied for the digestion. The PDSS undergoes a Thermal pressure hydrolysis (TPH) process (8 bar, 150 ~ 160 °C) prior to digestion. The third type of sludge, Digestate sludge (DS), originates from the Municipal Solid Waste Plant (MSWP) (Omrin, Netherlands).

Biomass bottom ash (BBA) and Al-anodizing waste (AAW) were utilized as additives in the mixture. The BBA was sourced from a local grate furnace, in which waste wood was incinerated for biomass fuel and the fly ash was removed in a cyclone. The AAW was obtained from a local WWTP that collects wastewater from the aluminum anodizing process in the alumina industry. The water glass powder with a composition of 20.1 wt% Na_2O and 62.7 wt% SiO_2 was employed, which has been reported to enhance reactive [SiO_2] content for gel formation and reduce the permeability [27]. Additionally, a mixture of 30 wt% blasting grit and 70 wt% normal sand was used as aggregate, both of which are considered inert, and their characterization tests are not included in this study.

2.2. Sample preparation

According to the Dutch legislation for the solid waste used in the soil layer, the proportion of the residue-based sealing layer is regulated to 46 wt% sludge, 9 wt% ash/filter, and 45 wt% sand fraction. The group labelled DSS-B denotes specimens prepared with DSS and BBA, while DSS-A represents specimens prepared with DSS and AAW. Additionally, all mixes are supplemented with 1.5 wt% water glass, based on previous

literature recommendations for its use in sealing materials within the range of 1–5 wt% [28]. The samples were externally prepared by Ingenieurbüro Kügler in Essen, Germany.

Based on the results of the optimal moisture content tests for each mixture (see details in Section 3.2), the grain and sludge materials were dried accordingly to ensure that each mix reached the optimum moisture content before molding. Subsequently, they were well dispersed in a laboratory mixer. BBA/AAW and water glass were gradually added while stirring to ensure uniform homogenization. Next, all the materials were cast into a cylinder mold (D = 95 mm, h = 50 mm) and compacted according to DIN 18127. The compacted blends (Fig. 2) were sealed in plastic bags for 70 days of curing at an ambient temperature.

2.3. Methodology

The flowchart of the process is presented in Fig. 2.

2.3.1. Characterization of raw materials

Raw materials were dried at 105 °C until a stable mass to determine their moisture content. A high-temperature furnace measured the weight loss between 105 and 1000 °C. The specific density of the dried materials was tested by using He-pycnometer (Accupyc II 1340 Micromeritics).

The particle size distribution of the raw materials was measured using a laser light scattering technique in isopropanol (Malvern Mastersizer 2000). To prevent agglomeration of sludge and AAW after drying, the test was conducted using wet raw materials, and 10 min of ultrasonic dispersion was performed beforehand. Due to relatively large particles in the BBA, sieve towers with 0.125, 0.25, 0.5, 1.0, 2.0, and 4.0 mm were employed to determine the particle size distribution.

The chemical compositions of raw materials was determined using X-ray fluorescence spectrometry (XRF) (PANalytical Epsilon 3). The borate fusion method was employed for the preparation of fused beads. The phase composition of raw materials was characterized by X-ray diffraction (XRD), Thermogravimetry (TG), and Fourier transform infrared spectroscopy (FT-IR). The XRD test was conducted by using a Bruker D4 phaser, with a step size of 0.02° and a 2θ range from 10° to 60° (Co-Kα, 40 kV, 30 mA). The TG test was carried out using a STA 449 F1 instrument for all materials at a heating rate of 10 K/min under the N_2 atmosphere. FT-IR spectroscopy was conducted by using Varian 3100 instrument to identify the bonding in the mineral phases with the wavenumber range of 4000–400 cm^{-1}.

The leaching behaviour of the raw materials was investigated following the one-batch leaching test (EN 12347–2). Raw materials smaller than 4 mm were mixed with distilled water in polyethene bottles at a liquid-to-solid (L/S) ratio of 10. The bottles were then sealed and placed horizontally on a linear reciprocating shaking device (Stuart SSL2) for 24 h, with a constant shaking rate of 250 rpm and an amplitude of 20 mm. Afterwards, the solids were filtered out, and the pH of the leachate was measured. The leachate was subsequently analyzed using ion chromatography (Dionex 1100) equipped with an ion-exchange column AS9-HS and inductively coupled plasma optical emission spectroscopy (ICP-OES Spectral Blue).

2.3.2. Characterization of the blends

The optimal water content of each mixture was determined according to the DIN 18127:2012–09 standard. The sludge materials were pre-dried at 40 °C for varying durations to adjust the water content of the initial material. Subsequently, all the raw materials were mixed and compacted. The cylindrical mould was filled with 3 kg of mixed samples, and each sample was prepared with three layers, each layer receiving 25 blows.

Permeability tests were conducted externally by Ingenieurbüro Kügler in Essen, Germany, following DIN18130 Part 1. The cylinder specimens, which had undergone 70 days of curing, were used for the permeability tests. These specimens were placed in a pressure cell with side pressure. The test duration was set at 75 days to ensure the stability of the permeability test results.

Phase assemblage characterization was conducted to identify the potential reaction products in all mixes. After 70 days of curing, the cylinder specimens were gently crushed and dried in a vacuum oven at 60 °C until constant weight. The dry samples were then sieved through a 63 μm sieve to remove the coarse aggregate and concentrate the reaction products for better analysis (Fig. 2). The fraction (< 63 μm) is a uniform grey powder. XRD, TG and FT-IR analysis of the finer fraction (< 63 μm) from each mixture was conducted as earlier mentioned. N_2 sorption analysis of the finer fraction (< 63 μm) was performed by using Micrometrics. The gel pore size distribution was calculated from the adsorption branch by the Barrett - Joyner - Hallenda method [29].

The micromorphology of the finer fraction (< 63 μm) were observed using Scanning Electron Microscope (SEM) and the chemical compositions of reaction products were analyzed with EDX (15KV) detector (Phenom Pro). The finer fraction (< 63 μm) was dried at 40 °C for 24 h and then coated with Au using a Quorum 150TS plus sputter coater.

The pore solution of each cylinder specimen after 70 days of curing was collected through pore solution expression, in which mechanical pressure was used to force the pore solution from the material. The pH of each pore solution was measured by a pH meter three times.

One-batch leaching tests were conducted on all specimens to evaluate heavy metal leaching. The testing and analysis procedures are detailed in Section 2.3.1.

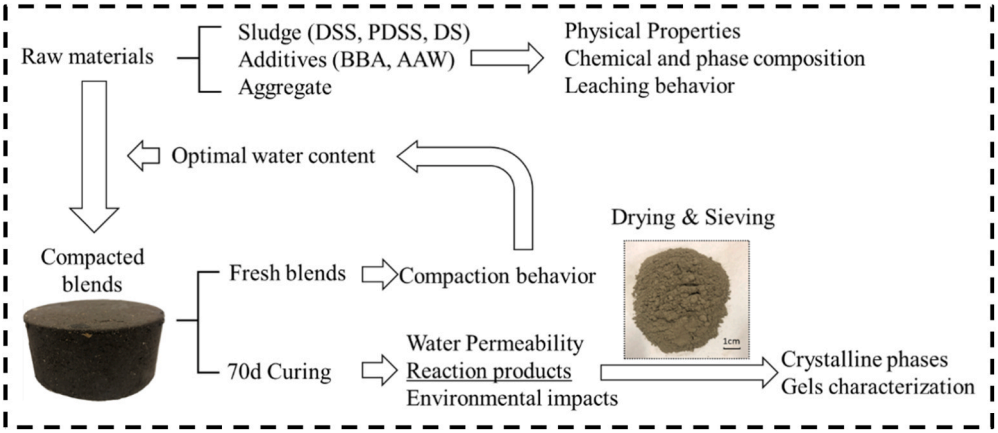

Fig. 2. Flowchart of the process for studying the sludge-based sealing materials.

3. Results and discussion

3.1. Physical and chemical properties of raw materials

The chemical compositions, moisture content and loss on ignition (LOI) of the raw materials are shown in Table 1. The sludge has a high moisture content and contains relatively high levels of iron sourced from the wastewater and the iron-based coagulants used during sewage treatment in the plants. The particle size distribution of all raw materials is shown in Fig. 3. DSS and PDSS exhibit a similar particle size distribution with a d50 of approximately 20 μm, indicating little influence on the particle size due to the TPH process. DS shows a larger particle size of around 30 μm, attributed to the lower soil content in the organic waste. BBA has an average particle size of 90 μm, while AAW has the smallest average particle size of around 11 μm.

The mineral composition of each raw material is characterized in Fig. 4. In the sludges, the presence of quartz (SiO_2 PDF#83–2465) and calcite ($CaCO_3$ PDF#72–1937) is observed, along with other minerals such as vivianite ($Fe_3(PO_4)_2{\cdot}(H_2O)_8$ PDF#75–1186) in DSS and chabazite-Na ($Na_{15.2}Al_{15.2}Si_{32.8}O_{96}$ PDF#83–1295) in PDSS. The broad diffused peaks between 20 and 30 (° 2θ) indicate a high organic content in the sludge. BBA consists of anhydrite ($CaSO_4$ PDF#72–0916), lime (CaO PDF#77–2010), calcite and quartz. AAW primarily contains boehmite (AlO(OH) PDF#49–0133), thenardite (Na_2SO_4 PDF#05–0631) and bayerite ($Al(OH)_3$ PDF#01–0287). The broad peaks of boehmite in AAW confirm its low crystallinity.

To further validate the findings from the XRD analysis, the FT-IR spectrum of each raw material is obtained and presented in Fig. 5. In the sludges, broad bands centred around 3245 cm^{-1} and 1630 cm^{-1} correspond to the stretching and bending vibrations of H-OH bonds [30]. The adsorption peaks at 2918 cm^{-1} and 2851 cm^{-1} can be attributed to the symmetric and asymmetric stretching bands of CH_2 [31], confirming the presence of organic content in the sludge materials. The adsorption peaks around 1416 cm^{-1} and 872 cm^{-1} represent the vibration of ν_3 [CO_3^{2-}] and ν_2 [CO_3^{2-}] in calcite, respectively [32]. The strong band around 1013 cm^{-1} may be due to the C-O stretching vibration from cellulose [31,33], but it is worth noting that the stretching vibration of the Si-O-Si bond in quartz or other silicates also absorbs this region [34]. In BBA, in addition to the adsorptions as mentioned above, the adsorption bands at around 1096 cm^{-1} and 648 cm^{-1} are attributed to the vibration of ν_3 [SO_4^{2-}] and ν_4 [SO_4^{2-}] from anhydrite [35]. Furthermore, strong adsorption around 3646 cm^{-1} is assigned to the vibration of hydroxyl groups, confirming the presence of lime in BBA [36]. AAW exhibits prominent adsorptions around 474 cm^{-1}, attributed to the [AlO_6] vibrations in boehmite [37].

Thermal analysis is performed to assess the volatile components in the raw materials, and the results are presented in Fig. 6. In the case of the sludges, the primary mass loss occurs between 250 and 500 °C, which is attributed to the decomposition of the organic compounds such as hemicellulose, cellulose, and the lignin present in the sludge [38]. Comparing DSS to PDSS, the pre-treatment of TPH leads to a slight decrease in organic content as high thermal pre-treatment may promote the transformation of organic content in PDSS from the particulate to the soluble fraction [39], whilst a significant reduction of organic compounds is observed in DS. The mass loss observed around 750 °C is associated with the decarbonation of calcite [40], which is also found in BBA. Regarding AAW, the initial mass loss occurs at around 105 °C, indicating moisture removal [41]. The subsequent mass loss between 250 and 400 °C is attributed to the dihydroxylation of interlayer OH in boehmite and bayerite [42].

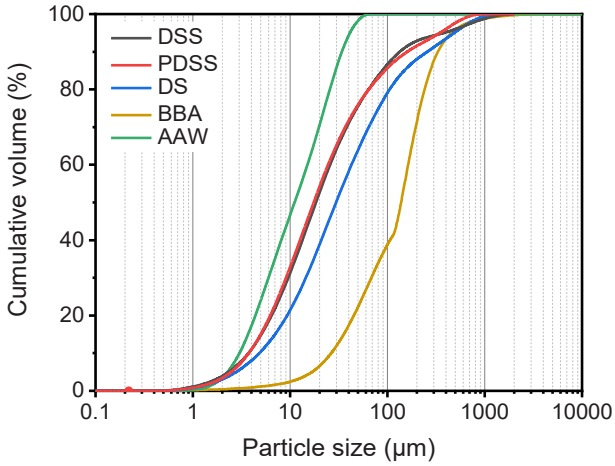

Fig. 3. Particle size distribution of each raw material.

3.2. Compaction behavior of the fresh blends

Compaction tests are conducted on each fresh blend to ensure the sealing materials achieve minimal void spaces after proper compaction, reducing the potential for leachate migration. The dry density vs. moisture content curves are presented in Fig. 7. The maximum dry density ($\gamma_{d\ max}$) of the fresh DS-B, PDSS-B, and DSS-B blends is 1.12 g/cm^3, 1.07 g/cm^3 and 0.95 g/cm^3, respectively. The corresponding optimum water content is 41.5 wt%, 44.4 wt%, and 56.4 wt%. The higher optimal water content in the DSS-B group indicates increased plasticity of the matrix prepared with DSS. This higher plasticity of the DSS-based matrix may be partially attributed to the higher organic content, as inferred by the TG results in Fig. 6, which can act as binding agents that enhance water retention [43]. On the other hand, using AAW in the sealing materials achieves a higher dry density than BBA. This enhancement can be associated with the finer particle size of AAW, which promotes better dispersion within the matrix.

Compacted blends were then prepared according to the optimal water content for each group of mixtures to ensure efficient compaction and achieve the lowest possible permeability. The following measurements are conducted with the compacted blends after 70 days of curing. The actual moisture content in the specimens after curing is listed in Table 2. Interestingly, the actual moisture content is lower than the optimal water because some water may evaporate during the mixing process and curing period. Besides, free water could be bounded into the newly formed minerals and gels during curing. Therefore, in addition to the geotechnical properties, reaction products also influence the microstructure of the sealing materials, as elaborated in more detail later.

Table 1
Chemical compositions of raw materials determined by XRF (wt%).

	DSS	PDSS	DS	BBA	AAW
Na_2O	0.1	0.1	0.1	0.2	4.2
MgO	0.9	0.5	1.1	1.6	-
Al_2O_3	0.7	1.3	2.4	2.5	55.2
SiO_2	2.6	2.0	11.2	20.8	0.8
P_2O_5	4.5	6.6	1.7	1.4	0.2
SO_3	1.9	2.3	2.9	5.8	11.8
K_2O	0.5	0.4	1.6	4.8	-
CaO	4.9	6.7	15.9	34.5	1.0
TiO_2	0.4	0.4	0.7	8.5	-
MnO	0.2	/	0.1	0.7	-
Fe_2O_3	18.1	16.4	13.8	7.2	0.6
ZnO	0.5	0.6	0.2	1.7	-
Cl	0.1	0.2	0.6	1.6	-
Others	0.4	0.5	0.2	1.6	2.4
Total LOI	64.2	62.0	47.5	7.1	23.8
Density (g/cm^3)	1.69	1.64	1.78	2.87	2.54

Moisture content and LOI are given in wt% (weight percentage).

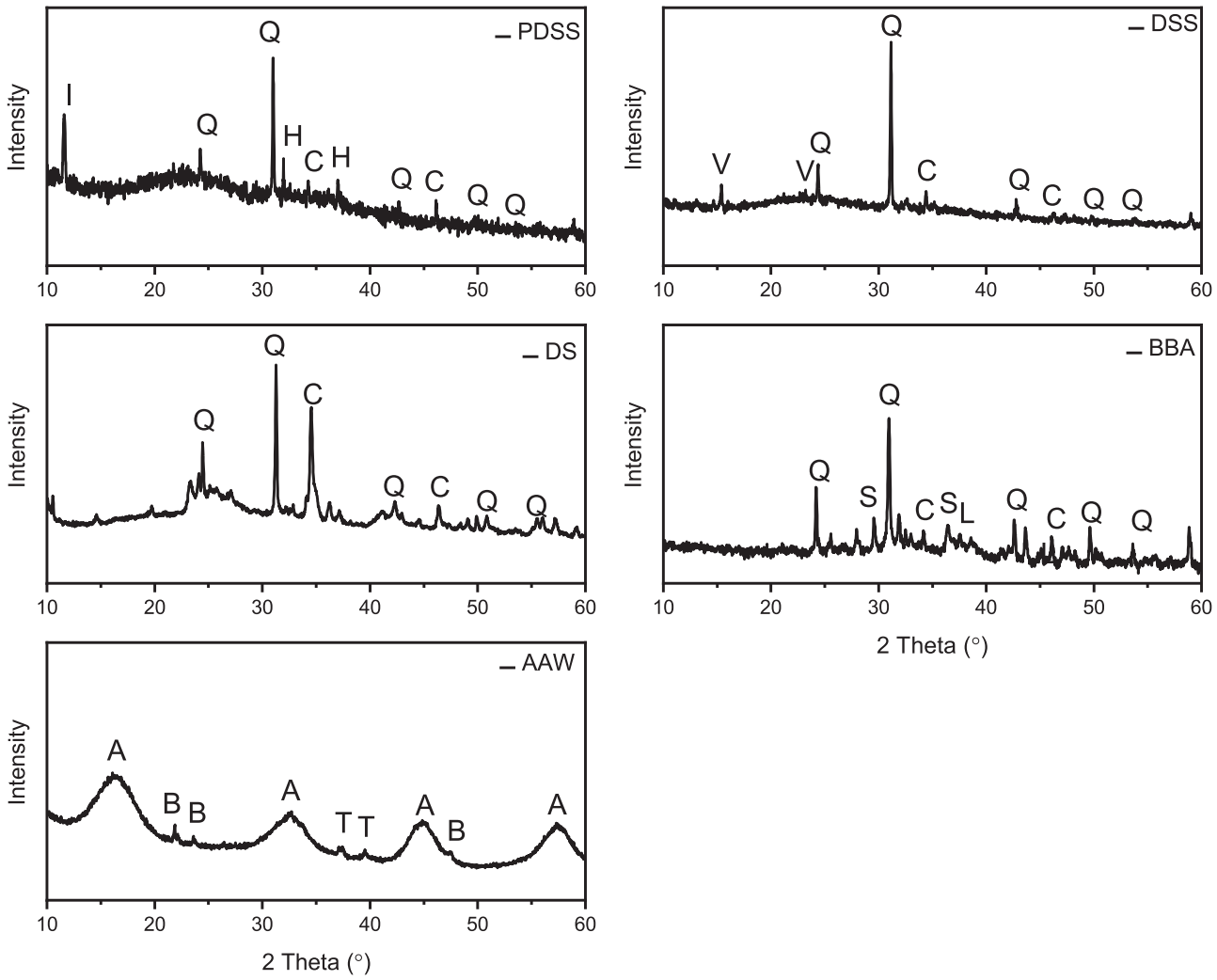

Fig. 4. XRD patterns of the raw materials. (A - boehmite: AlO(OH), B - bayerite: $Al(OH)_3$, C - calcite: $CaCO_3$, H - sodium chloride: NaCl, I - chabazite: $Na_{15.2}Al_{15.2}Si_{32.8}O_{96}$, L - lime: CaO, Q - quartz: SiO_2, S - anhydrite: $CaSO_4$, T - thenardite: Na_2SO_4, V - vivianite: $Fe_3(PO_4)_2$•8 H_2O).

3.3. Water permeability of the cured blends

Fig. 8 presents the permeability results of the cured samples, along with the limitation value indicated by the red line. The long-term impermeability requirement for a mineral sealing layer composed of landfill residues in the Netherlands is less than 20 mm/year, considering a layer thickness of 60 cm [44]. This legal requirement corresponds to a maximum k-value of 4.34×10^{-10} m/s for the sealing materials we designed. Overall, the k-values of the DSS and PDSS-based specimens satisfactorily meet the legislative requirements, while the DS-based specimens exhibit permeability slightly above the critical value. Therefore, the prepared DSS and PDSS-based sealing materials show promise for landfill applications in terms of impermeability. It is noteworthy that the lowest achieved permeability, approximately 3.78×10^{-12} m/s in DSS-A, falls below the majority of reported permeability values for sludge-modified sealing materials, which typically ranged from 1.0×10^{-4} - 1.2×10^{-11} m/s [9,45,46].

Regarding the effect of different sludge types, the permeability results are in agreement with the compaction curves presented in Fig. 7. With higher plasticity, the DSS-based blends effectively reduce the void spaces within the matrix after the compaction. Furthermore, the AAW-modified specimens exhibit lower permeability compared to the BBA-modified specimens. This improvement could be attributed to the finer particle size of AAW, which refines the pore size distribution of the matrix more effectively than BBA, confirming the positive effect of AAW as external gel products on permeability. Their potential contribution of the reaction products to the sealing materials will be further elucidated in the subsequent sections.

3.4. Reaction products characterization

3.4.1. Crystalline phases

The analysis of the reaction product composition focuses on the finer fraction below 63 μm of each sample, as it is expected to contain the highest amount of reaction products, while the larger fractions largely consist of inert aggregate. Fig. 9 (a) shows the XRD patterns of the sample prepared with different sludges and additives. Similar curves are observed, indicating that the different sludge and additives types have no significant influence on the formation of crystalline phases. The main crystalline phases identified include anhydrite ($CaSO_4$: PDF#72–0916), calcite ($CaCO_3$:PDF#72–1937), gypsum ($CaSO_4$•2 H_2O: PDF#33–0311), sodium chloride (NaCl: PDF#70–2509) and quartz (SiO_2: PDF#83–2465). Additionally, some other minerals, such as Vivianite ($Fe_3(PO_4)_2{\cdot}(H_2O)_8$: PDF#75–1186) and Chabazite-Na ($Na_{15.2}Al_{15.2}Si_{32.8}O_{96}$: PDF#83–1295), originate from the raw materials DSS and PDSS, respectively.

Meanwhile, the formation of the gypsum in the mixture is confirmed through the FT-IR spectrums in Fig. 9 (b). The band adsorptions at around 3536 cm^{-1}, 3392 cm^{-1} and 1675 cm^{-1} are assigned to the stretching vibration peaks of the hydroxyl group, while the peaks at

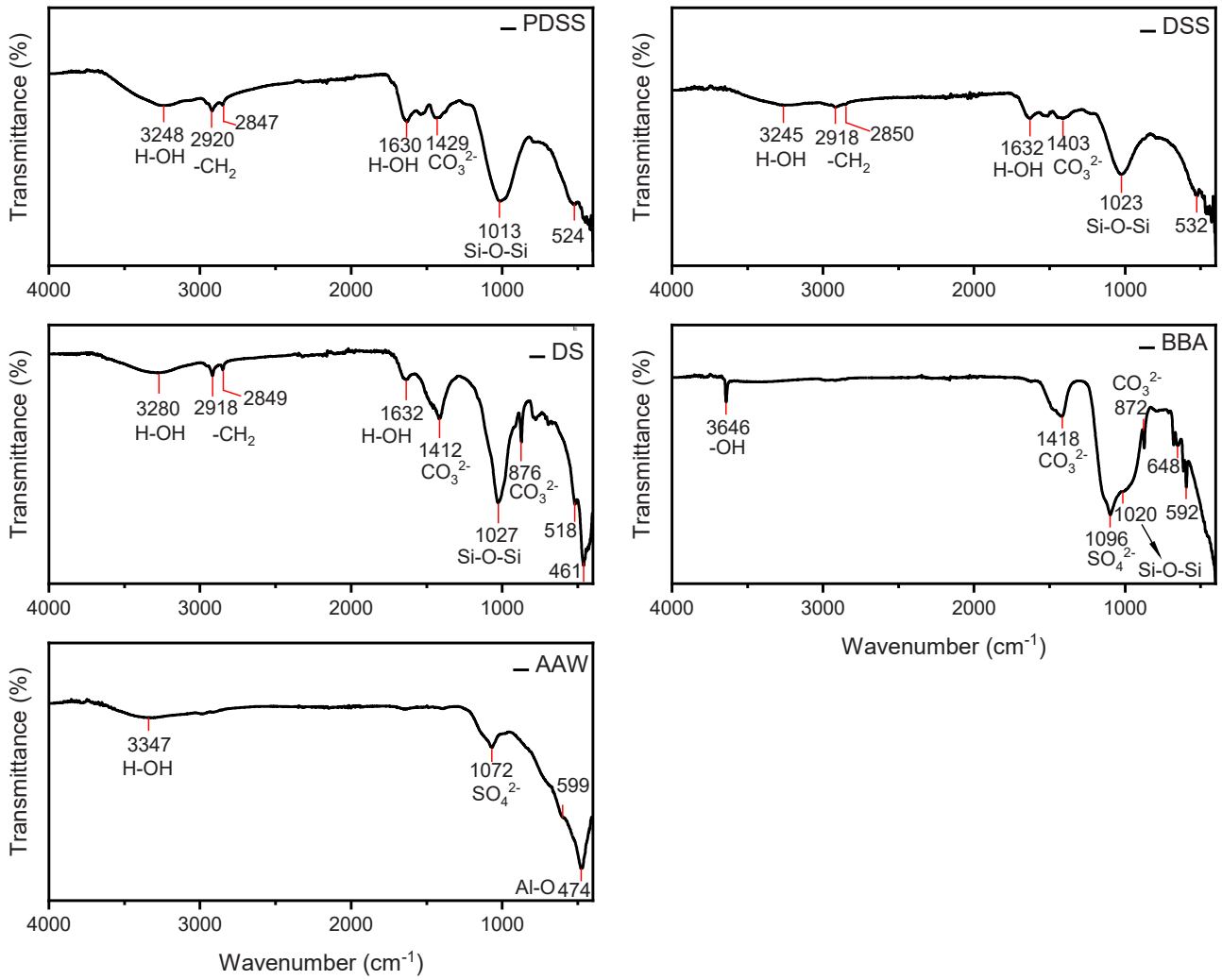

Fig. 5. FT-IR spectra of the raw materials.

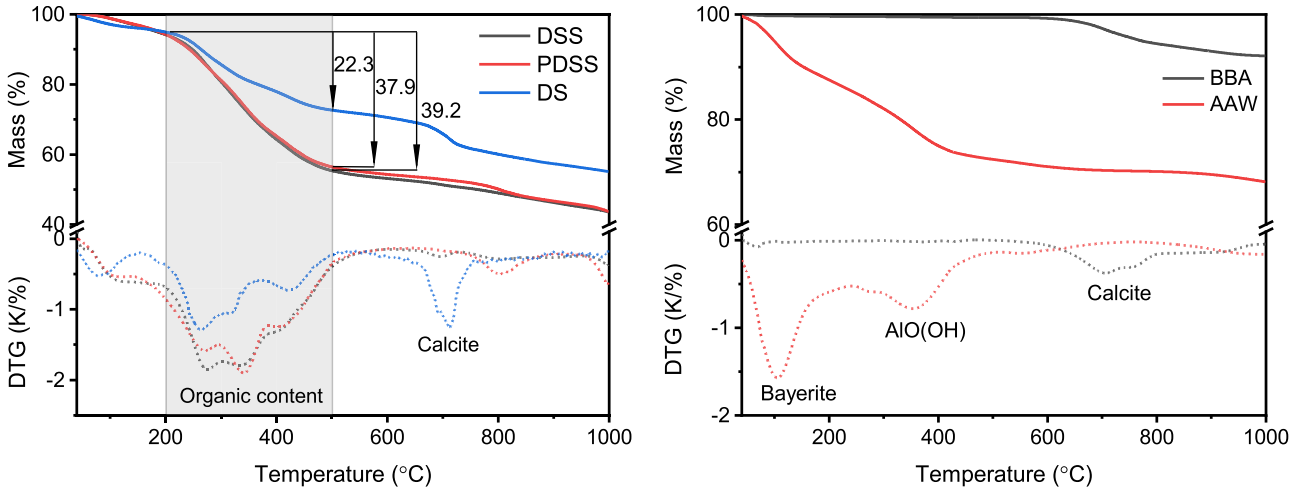

Fig. 6. TG and DTG curves of the raw materials (Left: sludges, Right: additives).

1614 cm^{-1} and 1118 cm^{-1} are attributed to the stretching vibration of S-O and S═O, respectively [47]. The peaks at 667 cm^{-1} and 599 cm^{-1} represent the stretching and bending vibration of sulfate [48]. The C-O stretching and bending vibrations around 1425 cm^{-1} and 865 cm^{-1} are identified due to the presence of the calcite. A slight difference in the adsorption peak of 1022 cm^{-1} is observed among all FT-IR spectrums. It is noteworthy that both C-O stretching vibration from the cellulose structure (organic content in sludge) and Si(Al-O) vibrations from silicates/aluminates (e.g. quartz, silica gel, calcium silicate hydrate gel) can contribute to this band [49,50]. Further details about the formation of

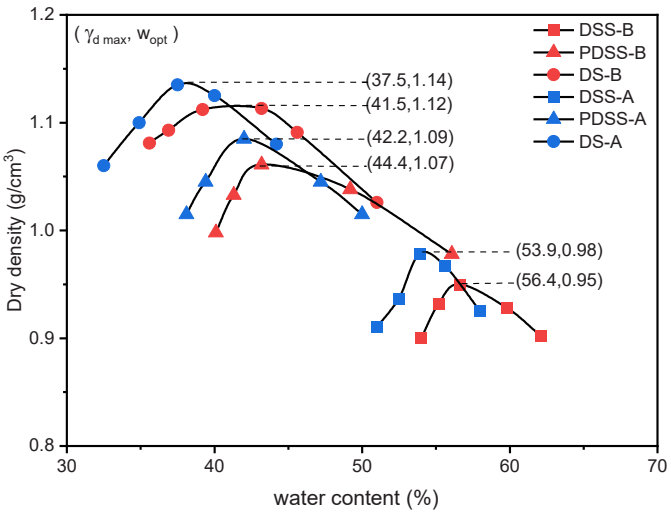

Fig. 7. Compaction curves for each mix (γ_{dmax} - Maximum dry density, w_{opt} - Optimal water content).

Table 2
The actual moisture content in specimens after 70 days of curing.

Group ID	DSS-B	DSS-A	PDSS-B	PDSS-A	DS-B	DS-A
Actual moisture %	36.4 (± 1.5)	41.8 (± 0.8)	34.1 (± 1.2)	36.8 (± 2.0)	30.6 (± 1.1)	34.9 (± 0.7)

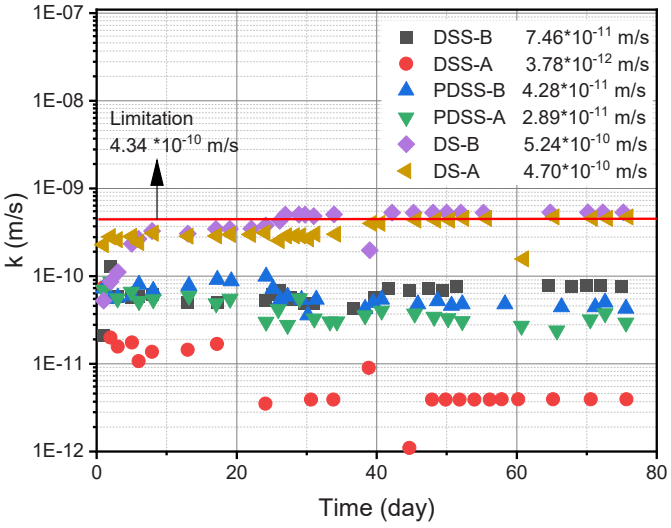

Fig. 8. The permeability test of the sludge-based landfill cover samples within 70 d. The red line represents the impermeability requirement in the Netherlands.

gels are illustrated in Section 3.4.2.

TGA tests were performed on all samples to evaluate the formed gypsum amount, and the results are presented in Fig. 9 (c-e). The TG curves show two major mass losses around 110 - 180 °C and 600 - 800 °C, which could be attributed to the dehydration of gypsum and the decarbonation of the calcite [40,51]. Each mass loss is then calculated based on the tangential method [52], and the results are labelled in the figures. Interestingly, the AAW-modified specimens show a higher formation of gypsum than the BBA-modified specimens. This could be explained by the presence of thenardite in AAW, which contributes to a higher sulphate leaching than anhydrite in BBA (see details in Section 3.5). Besides, a slight mass loss peak around 85–105 °C is observed in the DTG curves of all specimens, which is associated with the dehydration of the gel products. The AAW-modified specimens exhibit a higher mass loss than the BBA-modified specimens for this peak, which could be accounted for by the bound water in AAW, as depicted in Fig. 6.

In conclusion, gypsum and gel products are the main new phases detected in the established sealing materials. As indicated by the TG-DTG curves in BBA-modified and AAW-modified specimens, the gypsum content is related to the leachable sulfate content in each mix, and the low bound water content indicates the relatively low formation of gel content. Meanwhile, the transformation of free water into bound water explains the described reduction in moisture content of the matrix presented in Table 2.

3.4.2. *Amorphous phases*

N_2 adsorption (BET) of the finer fraction (below 63 μm) from each mix, alongside the raw BBA and AAW, was performed to examine the formation of gel products further, as presented in Fig. 10. In terms of pore size, gel pores (less than 10 nm) and capillary pores (10 ~ 100 nm) are the two main classes of pores [53]. For the raw materials, two maxima around 3 nm and 7 nm are observed in the raw AAW, whereas no gel pores are observed in the raw BBA. The main component of AAW is colloidal boehmite with very low crystallinity (see Fig. 4). It has been reported that the porosity of colloidal boehmite is ultimately correlated with its crystallite size [41]. Hence, colloidal boehmite is likely present in two different particle sizes in the raw materials AAW.

Regarding the cured blends, the AAW-modified specimens exhibit a higher total pore volume than the BBA-modified specimens, likely due to the presence of higher gel pores in raw AAW. Nevertheless, one of the maxima at around 3 nm disappears in the AAW-modified specimens, indicating the potential reaction of colloidal boehmite or the crystallization of colloidal boehmite over time. On the other hand, the BBA-modified specimens show relatively lower gel pore volumes, consistent with the TG results, suggesting the lower formation of gel products. It is important to note that while gel pores increase the total porosity of the matrix, they do not increase the permeability [53]. Instead, an abundance of gel pores in the matrix indicates higher gel contents that can fill the larger porosity and reduce permeability [54]. Therefore, the lower permeability of AAW-modified specimens could be attributed to the increased gels sourced from AAW, while BBA-modified specimens exhibit less gel formation.

The effects of BBA and AAW on the gel composition of the specimens were further investigated. The finer fraction (below 63 μm) from DSS-B and DSS-A was subjected to SEM analysis with backscattered electron imaging, and the elemental composition was studied using EDX mapping. Fig. 11 displays the observed particles, including organic fibers, gypsum, and quartz. Analyzing the mapping results of DSS-B specimens in Fig. 11 (a), it is evident that the distribution of Ca element is primarily influenced by the presence of gypsum. Interestingly, despite the expected formation of C-S-H gel resulting from the reaction between lime (from BBA) and water glass [55], there is no observed correlation between elemental Ca and Si in the mapping results. This lack of correlation may be attributed to interference from the composition of gypsum and quartz or suggest that the resulting C-S-H gel has decomposed due to the low alkalinity of the environment. Table 3 presents the pH value of the pore solution obtained by compressing the cured specimens, indicating that the C-S-H gel is not stable in such an environment, as the pH value is close to neutrality [56]. This instability is likely due to the low dosage of lime-containing BBA used, which might not have provided sufficient alkalinity to stabilize the C-S-H gel. The reduced gel pore volume in the BBA-modified specimens further supports this observation. It should be noted that over time, the C-S-H gel may undergo decomposition through carbonation, leading to increased permeability of the matrix [57]. Based on the hydrolysis properties of waterglass in a neutral environment, the main product of the reaction appears to be silica gel, which exhibits resistance to carbonation [58]. Consequently, it can be inferred that silica gel serves as the primary gel product in

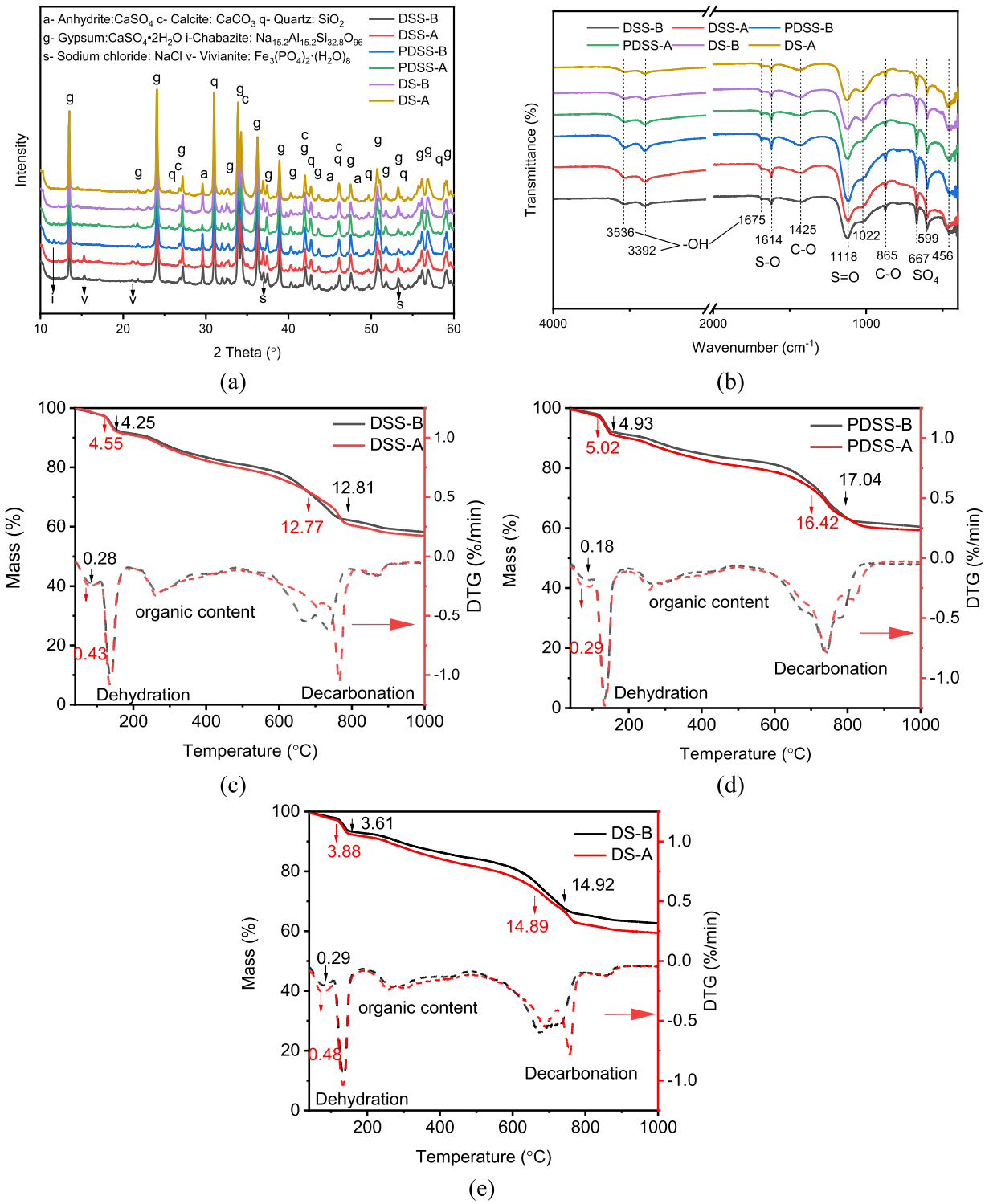

Fig. 9. (a) XRD patterns, (b) FT-IR spectrum and (c-e) TG-DTG curves of the finer fraction (below 63 μm) from each mix.

BBA-modified specimens and offers advantages in terms of stability.

According to N_2 adsorption behaviour, the gel pores observed in AAW-modified specimens are related to colloidal boehmite in AAW. Consequently, three particles with high Al content in the mapping results in Figure 11 (b) were selected for further spot analysis. Ten spots were tested for each particle, detecting elements including Na, Si, Mg, Ca and S. The average mass proportion of these elements is calculated and presented in Table 4. When compared with the XRF bulk compositions of the raw AAW, the three particles exhibit a decrease in Al_2O_3 content. The SO_3 content in these particles also varies due to the high mobility and leaching of sulphate (Na_2SO_4) from AAW. However, a portion of the leached sulphate is partially redeposited as the precipitation of anhydrite/gypsum, as confirmed by the increased CaO content within the three particles. Overall, the relatively low CaO, Na_2O and MgO contents indicate the absence of C/N-(A)-S-H gel or M-S-H gel formation. The relatively high SiO_2 content is likely originating from the dissolved water glass, also evidencing the formation silica gel. In conclusion, the main gel products in the AAW-modified specimens are

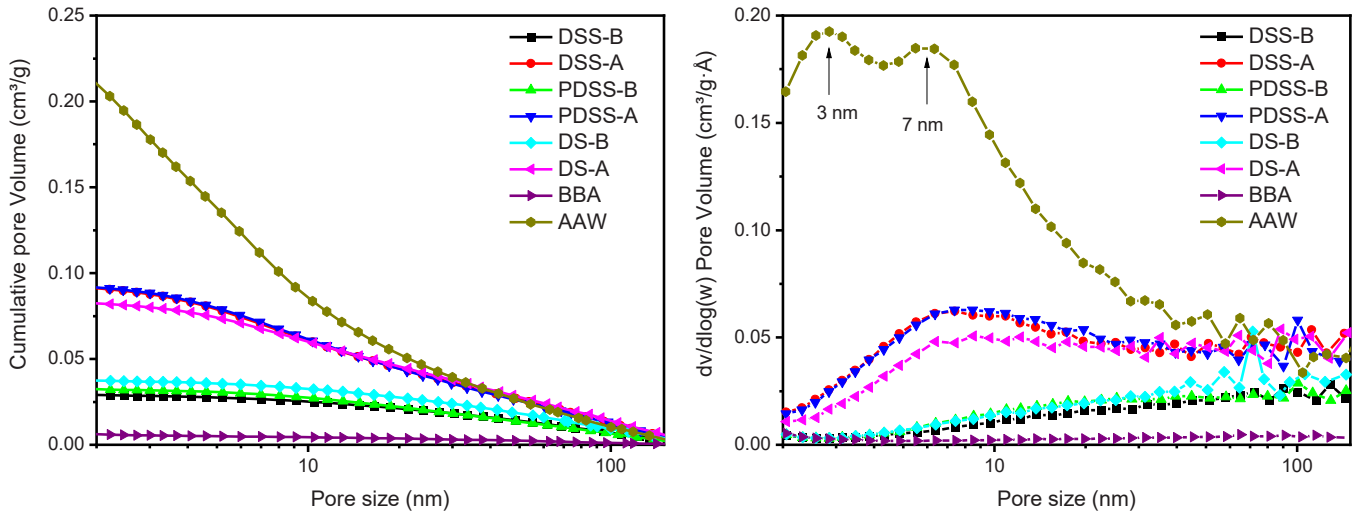

Fig. 10. N_2 adsorption behaviour of the finer fraction (below 63 μm) from each group and raw materials BBA and AAW: left - Cumulative pore volume, right - Pore size distribution.

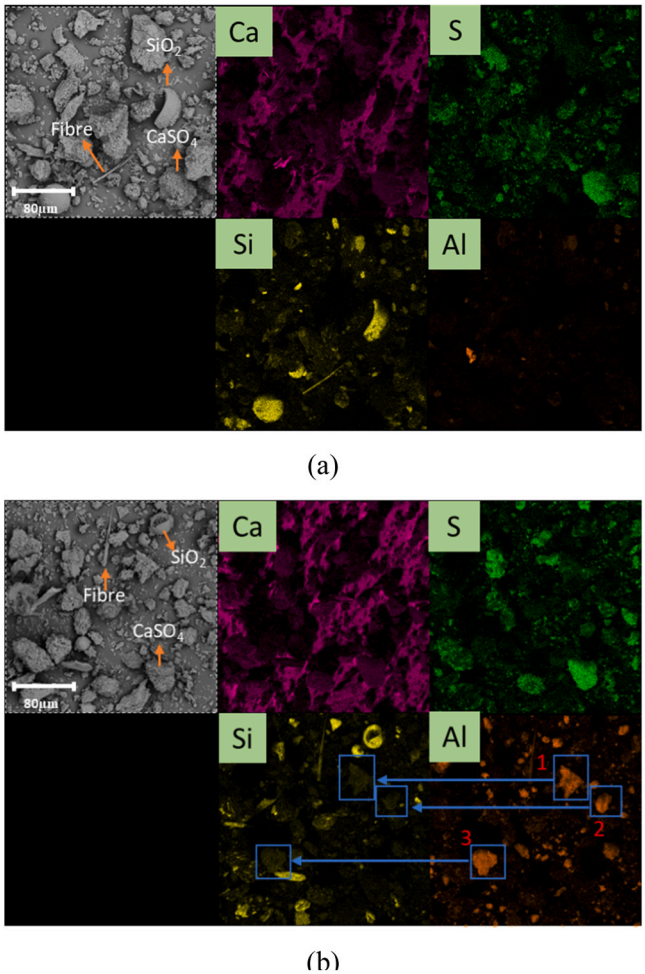

Fig. 11. EDS mapping of (a): DSS-B and (b): DSS-A, including BSE image. (Three particles rich in Al element are marked 1, 2, and 3, further analyzed with EDX spot analysis.).

Table 3
pH measurement of the pore solutions of all cured specimens.

Group	DSS-B	DSS-A	PDSS-B	PDSS-A	DS-B	DS-A
pH	8.2 ± 0.2	8.2 ± 0.1	8.2 ± 0.2	7.8 ± 0.3	8.3 ± 0.1	8.2 ± 0.1

Note: After 70 days of curing, the pore solution of each specimen is obtained by compression. pH of the pore solution is then measured using a pH meter.

Table 4
The element composition of three Al-rich particles from the DSS-A sample in Fig. 11 and the raw material AAW from XRF analysis.

Mass proportion %	Particle 1	Particle 2	Particle 3	AAW
Al_2O_3	61.0 ± 2.9	66.9 ± 2.3	66.9 ± 1.4	75.6
SiO_2	19.2 ± 1.6	17.1 ± 1.4	17.1 ± 2.3	1.1
Na_2O	5.7 ± 2.0	4.0 ± 0.9	4.1 ± 0.6	5.8
SO_3	7.6 ± 1.7	5.9 ± 1.7	5.0 ± 0.5	16.2
CaO	3.8 ± 1.0	3.7 ± 1.9	2.8 ± 0.4	1.4
MgO	2.6 ± 0.2	2.5 ± 0.2	4.1 ± 1.2	-

Note: " - " means no Mg element in raw AAW. Ten spots for each particle are collected, and the average values are calculated.

the original colloidal boehmite and the formed silica gel, and the nature of the bonding between them remains unclear.

3.5. Environmental impact

In principle, landfills are designed with leachate collection systems to minimize the impact of the landfills on the environment and surrounding communities. In a practical application in the Netherlands, a 2 mm HDPE layer will be installed on the top of the sealing layer. The purpose of this HDPE layer is to prevent rainwater infiltration (see Fig. 1) and to separate the vegetation layer from the sealing layer. This also allows for the utilization of industrial by-products as sealing material. In this work, the leaching behavior of both the raw materials and the prepared sealing materials was tested to mitigate its environmental impact in the event of unanticipated damage to the HDPE layer during installation or after prolonged use.

3.5.1. Leaching behavior of raw materials

The chemical compositions of the leachates obtained from the raw materials, in comparison with the respective limit values for disposal in landfills, is presented in Table 5. The leachable elements in the sludge

Table 5
The leaching of all materials obtained via a one-batch leaching test in comparison with disposal limits for non-hazardous materials (mg/kg dry materials, UDL for under detection limits).

Raw material	DSS	PDSS	DS	BBA	AAW	Disposal Limits
Chloride	830	660	860	4590	3490	15000
Sulfate	2120	2730	380	19270	**69910**	20000
As	**2.65**	1.55	0.51	UDL	0.04	2
Ni	3.85	3	0.58	UDL	UDL	10
Pb	4.25	3.3	UDL	**304.4**	0.12	10
Zn	1.75	1.45	0.40	28.95	0.01	50
Ba	0.15	0.15	0.07	1.76	0.05	100
Cr	0.2	0.1	0.05	**25.39**	0.79	1
Cu	1.2	1.65	UDL	0.16	0.05	10
Mo	1.7	2.5	0.19	3.28	0.17	50
Sb	0.2	0.25	UDL	UDL	0.04	10
B	3.1	5	2.38	2.85	45250	-
Fe	38.4	52.2	2.19	UDL	UDL	-
Mg	486.8	196.1	114	0.03	13.28	-
Mn	0.7	0.35	0.12	UDL	0.04	-
Sr	1.95	1.45	1.62	40.46	0.73	-
Nitrate	7.9	18	UDL	UDL	UDL	-
Phosphate	100	100	UDL	UDL	UDL	-
NH_4^+	1550	980	1900	UDL	UDL	-
Na^+	960	830	720	2480	41280	-
K^+	540	310	540	6070	24	-
Ca^{2+}	460	390	330	6120	133	-
Al^{3+}	5	8.1	0.20	0.08	0.46	-
pH	8.14	8.07	8.31	12.93	8.39	-

materials include the heavy metals As, Ni, Pb, Zn, Cu, Mo and Fe, as well as the alkali metals Na, K, Ca and Mg. The BBA exhibits high leaching levels of sulfate and Ca due to the anhydrite and lime. Heavy metals such as Pb, Zn and Cr are also observed in the leachate of BBA. As for the AAW, the leachate comprises the sulphate and Na due to the Na_2SO_4. Overall, the leaching level of As in the DSS, Pb and Cr in the BBA, and sulfate in the AAW exceed landfill disposal limits for non-hazardous materials. Consequently, further leaching tests of the cured specimens focus on the above heavy metal ions and sulfate anions.

3.5.2. *Leaching of the cured blends*

Fig. 12 presents a summary of the leachable content of sulphate, As, Cr and Pb from the cured specimens, determined through one-batch leaching analyses. The immobilization rate of each element is expressed by:

$$\gamma = \sum M_C \times m_i \times L_i$$

$$\alpha = (1 - \frac{M_C \times L_C}{\gamma}) \times 100\%$$

Where γ represents the theoretical maximum leachable content in each cured specimen (mg), M_C is the mass of the cured specimen (kg), m_i is the mass proportion of component i (i.e., sludge or additives) (%), L_i denotes the leachable elements in component i (mg/kg), L_C refers to the leachable elements in the cured specimen (mg/kg), α represents the immobilization rate of the element in the cured specimens (%).

It is essential to note that the one-batch leaching test employs a L/S ratio of 10, with crushed solid particles below 4 mm in size. This approach enables the measurement of potentially leachable ions and eliminates the need for simulating the process of a compacted seal being flushed through rainwater to obtain the filtrate. Overall, all cured blends exhibit desirable leaching levels for sulphate (< 20000 mg/kg), As (<2 mg/kg), Cr (<1 mg/kg) and Pb (< 10 mg/kg), indicating the absence of heavy metal pollution concerns in the prepared sealing

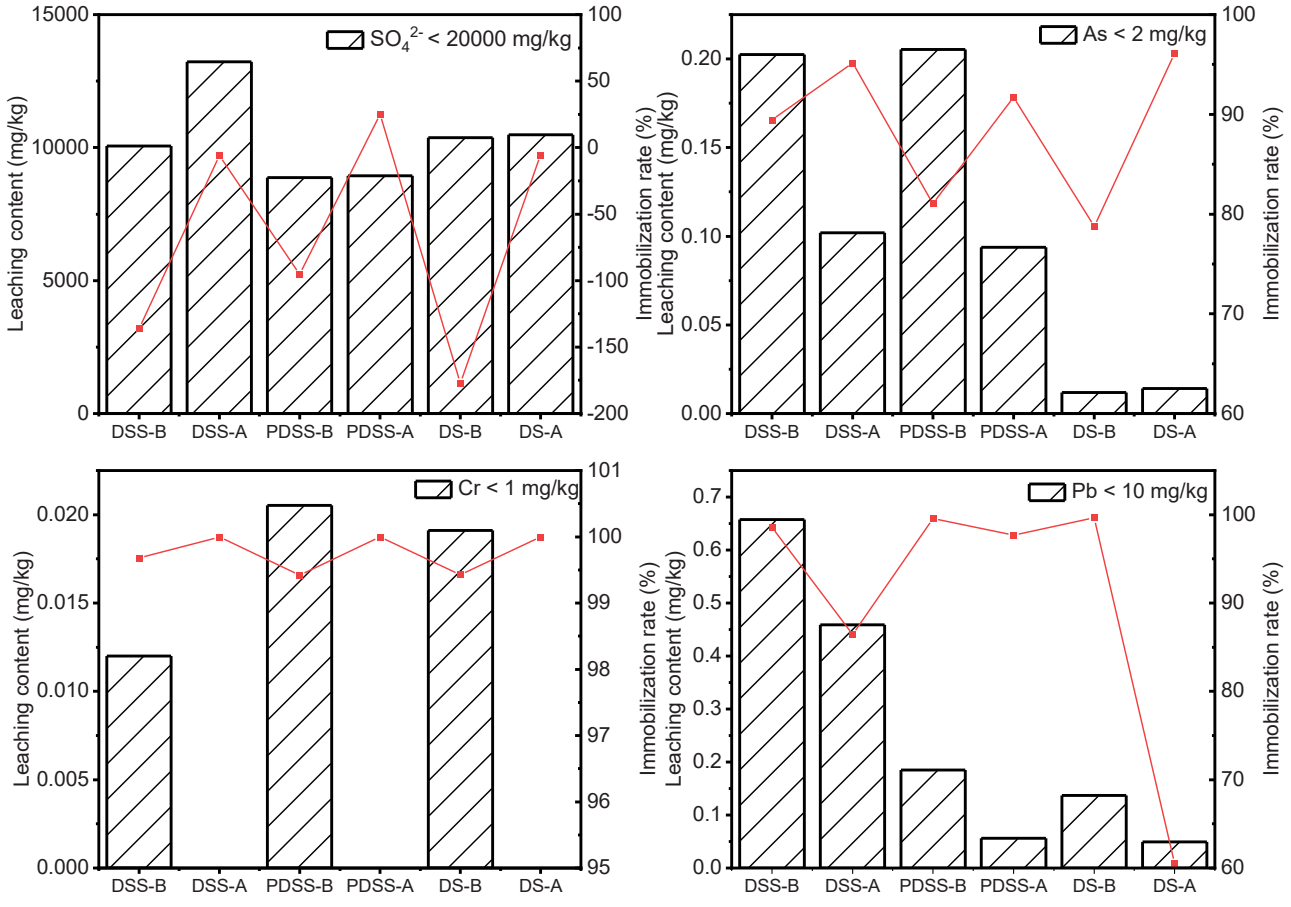

Fig. 12. Leaching content of the sulphate, As, Cr, and Pb from the cured specimens (mg/kg dried materials).

materials. The relatively higher sulphate leaching in all blends is primarily attributed to the solubility of gypsum (~2 g/L, 25 °C), as confirmed by the XRD patterns shown in Fig. 9. It also explains the observed regressive sulphate immobilization rates in the cured specimens.

The leaching of As, mainly originating from the sludge DSS and PDSS, is observed in the DSS-based and PDSS-based specimens. Incorporating AAW, in comparison to BBA, reduces the leached As content. This enhanced immobilization rate of As is likely attributed to higher leached sulphate from AAW. As ferrous sulfate and aluminum sulfate are commonly used coagulation agents to remove As [59], a similar effect may be achieved because of the sufficient iron and sulfate content in the sealing materials. In the case of Cr leaching, it is only observed in the BBA-modified specimens, as Cr primarily originates from the raw BBA. According to the study on Cr leaching behavior in soil by Weng et al. [60], the lower leaching content of Cr in DSS-based specimens is associated with the higher organic content in the DSS (Fig. 9). Pb leaching is mainly from DSS and BBA, resulting in the highest Pb leaching from DSS-B. However, most cured specimens show a desirable immobilization rate of Pb. Leachable Pb is often stabilized as the silicate species, as reported by [61]. Thus, the 1.5 wt% water glass is sufficient for the precipitation of $PbSiO_3$. Notably, some previous studies have reported the effect of organic content on absorbing the Pb [62,63]. In summary, the high immobilization of heavy metal ensures no soil pollution occurs in the landfill cover system.

3.6. Benefits and limits discussion

The installation of a landfill cover system is crucial for landfill closure. As depicted in Fig. 13, the Netherlands has a significant number of operational landfills [64]. When these landfills approach full capacity in the future, a substantial amount of sealing material will be required for their closure. By utilizing sludge from WWTPs, raw material costs can be reduced, and the ecological impact of clay excavation can be eliminated. This approach also enables the sustainable recycling of industrial by-products, making it a more environmentally friendly alternative to using excavated clay. In the Netherlands, the annual production of DSS, PDSS and DS from WWTPs and MSWPs is 1400, 20, and 50 metric tons, respectively. These solid waste resources offer a sufficient and economical supply of sealing materials for landfill closure without compromising the primary objective of effective waste containment.

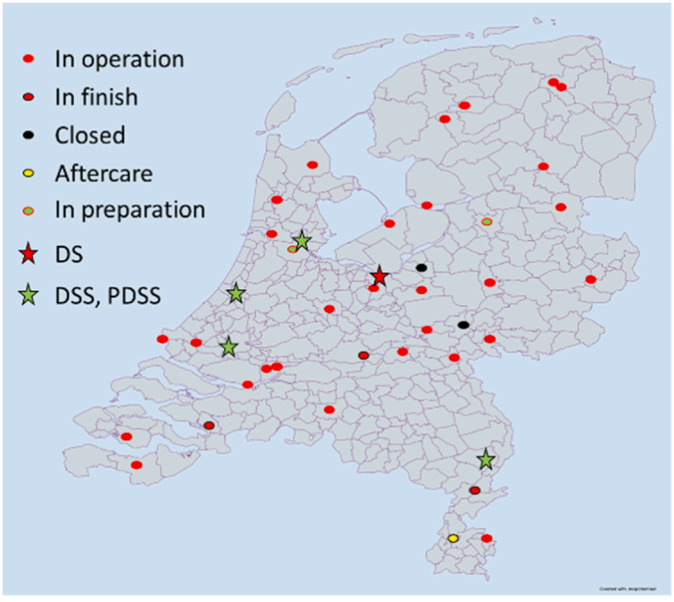

Fig. 13. Overview of landfills and WWTPs in the Netherlands. (The map is created with mapchart.net)

The toxicity of industrial solid waste is often criticized for its high-leached heavy metals, leading to high waste management costs. However, applying BBA in sludge-based sealing materials can effectively utilize the organic content in the sludge to adsorb Pb and Cr from BBA. On the other hand, the highly leached sulfate in AAW and BBA is stabilized as the gypsum in the sealing materials, filling voids and further improving the impermeability along with the original amorphous boehmite and the formed silica gel. Moreover, the high sulphate concentration facilitates the adsorption of As from the sludge [59]. The heavy metals are effectively stabilized in the sealing material. This approach offers new insights into the solidification of heavy metals-containing solid waste within the sealing materials. It is important to note that HDPE separates the sealing layer from the vegetation layers above, thereby preventing the heavy metal contamination of the upper soil. Meanwhile, it also indicates the application limitations of this sealing material, i.e. the corresponding protective HDPE are required.

The fact that the permeability of the DS-based specimen is slightly outside the limits does not necessarily exclude DS as a viable raw material for sealing materials. Various factors influence permeability, including mix design, additives, and compaction degree. For instance, incorporating AAW can effectively reduce the permeability of a sealing material compared to using BBA. Hence, optimizing the sealing material properties by adjusting the mixing ratios to meet regulatory requirements is possible. These considerations are beyond the scope of the study at this stage, but related investigations will be conducted in future research. This research was done in laboratory conditions. Future work is also required to be done in large-scale and field tests.

4. Conclusions

The work aims to co-product low-permeable sealing materials for final landfill cover systems by utilizing industrial solid waste. Various industrial products, including DSS, PDSS, DS, BBA and AAW from WWTPs and MSWPs, have been selected and characterized for this purpose. The study explores the effect of different types of sludge on sealing performance and investigates the influence of various additives on gel formation within the blends. Furthermore, the potential environmental impact of the prepared sealing materials is revealed through their leaching behavior. Based on the obtained results, the following conclusions can be drawn.

The sealing materials derived from industrial by-products have achieved low permeability, with DSS-A showing the optimal permeability, boasting a k-value of 3.78×10^{-12} m/s. Despite a slight degradation in permeability caused by the pre-treatment of TPH, PDSS-based specimens still comply with Dutch requirements for soil capping, highlighting its potential as a sustainable end-of-life solution. However, the permeability of DS-based specimens slightly exceeds the requirements due to the relatively lower organic content in DS.

The primary reaction product in the sealing materials is gypsum, which is attributed to the high leachable sulphate from the BBA and AAW. Considering the low pH of the pore solution in the BBA-modified specimens, the addition of water glass is expected to result in the formation of silica gel rather than the C-S-H gel. On the other hand, AAW proves to be an effective external gel, providing the desired permeability for AAW-modified specimens. The colloidal boehmite in AAW remains stable and behaves similarly to the gel products, effectively filling the voids and reducing the porosity.

The heavy metals from the industrial by-products are well immobilized in the sealing materials. The reduction of As leaching from DSS is attributed to the coagulation of sulphates. The leachable Cr from BBA is adsorbed in the organic content in the sludge, whereas Pb is stabilized as the $PbSiO_3$. There are no heavy metal pollution concerns in the sludge-based sealing materials.

This work represents a significant advancement in recycling

industrial by-products for landfill cover construction. The proposed novel approach to sustainable landfill sealing materials presents promising applications in the Netherlands, offering advantages in terms of cost, reduced environmental impact, and the valorization of industrial by-products.

CRediT authorship contribution statement

Chen Wei: Supervision, Project administration. **Schollbach Katrin:** Writing – review & editing, Supervision, Conceptualization. **Ling Xuan:** Writing – original draft, Visualization, Validation, Methodology, Investigation, Formal analysis, Conceptualization. **Brouwers H.J.H.:** Writing – review & editing, Supervision, Project administration, Funding acquisition.

Declaration of Competing Interest

The authors declare that they have no known competing financial interests or personal relationships that could have appeared to influence the work reported in this paper.

Data availability

Data will be made available on request.

Acknowledgements

This research was carried out under project number T20014 in the framework of the Research Program of the Materials innovation institute (M2i) (www.m2i.nl), supported by the Dutch government. This research was also supported by the funding of the China Scholarship Council (No. 201906950015) and the Eindhoven University of Technology. The authors would like to thank Euro Trust Management for supplying all raw materials and the Ingenieurbüro Kügler for the experimental tests. The discussion with Mr J. Winter (ETM), Mr H. Beukema (ETM) and Mr J. Steketee (TAUW) is appreciated.

References

[1] W.Y. Lin, W.C. Ng, B.S.E. Wong, S.L.M. Teo, G. d/o Sivananthan, G.H. Baeg, Y. S. Ok, C.H. Wang, Evaluation of sewage sludge incineration ash as a potential land reclamation material, J. Hazard. Mater. 357 (2018) 63–72, https://doi.org/10.1016/j.jhazmat.2018.05.047.

[2] J. Namie, P. Konieczka, Review of sewage sludge management: standards, regulations and analytical methods, J. Clean. Prod. 90 (2015) 1–15, https://doi.org/10.1016/j.jclepro.2014.11.031.

[3] D. Sandy, Final Implementation Report for Directive 86/278/EEC on Sewage Sludge: 2013 – 2015, Portugal, 2018. ⟨https://policycommons.net/artifacts/1976397/final-implementation-report-for-directive-86278eec-on-sewage-sludge/2728162/⟩ on 19 Jun 2023.

[4] S.N. (CBS), Urban waste water treatment per province and river basin district 2020, 2023. ⟨https://opendata.cbs.nl/#/CBS/en/dataset/7477eng/table?dl=91C32⟩ (accessed June 16, 2023).

[5] K. Taki, S. Choudhary, S. Gupta, M. Kumar, Enhancement of geotechnical properties of municipal sewage sludge for sustainable utilization as engineering construction material, J. Clean. Prod. 251 (2020) 119723, https://doi.org/10.1016/J.JCLEPRO.2019.119723.

[6] A.A. Brian, H.B. Craig, Effect of desiccation on compacted natural clays, J. Geotech. Geoenviron. Eng. 127 (2001) 67–75, https://doi.org/10.1061/(ASCE)1090-0241(2001)127:1(67).

[7] D. Koch, Bentonites as a basic material for technical base liners and site encapsulation cut-off walls, Appl. Clay Sci. 21 (2002) 1–11, https://doi.org/10.1016/S0169-1317(01)00087-4.

[8] Q. Xue, Y.C. Lei, Erosion characteristics of ecological sludge evapotranspiration cover slopes for landfill closure, Environ. Earth Sci. 75 (2016) 1–8, https://doi.org/10.1007/s12665-015-5166-0.

[9] I. Herrmann, M. Svensson, H. Ecke, J. Kumpiene, C. Maurice, L. Andreas, A. Lagerkvist, Hydraulic conductivity of fly ash–sewage sludge mixes for use in landfill cover liners, Water Res 43 (2009) 3541–3547, https://doi.org/10.1016/J.WATRES.2009.04.052.

[10] N.A. Rosli, H.A. Aziz, M.R. Selamat, L.L.P. Lim, M.H. Zawawi, Effect of compaction on physical properties of a sewage sludge and red gypsum mixture as intermediate landfill cover, Constr. Build. Mater. 289 (2021) 123153, https://doi.org/10.1016/J.CONBUILDMAT.2021.123153.

[11] M.P. Carignan, C.B. Lake, T. Menzies, Assessment of two thermally treated drill mud wastes for landfill containment applications, Waste Manag. Res. 25 (2007) 394–401, https://doi.org/10.1177/0734242×07073652.

[12] M. Fall, J.C. Célestin, F.S. Han, Suitability of bentonite-paste tailings mixtures as engineering barrier material for mine waste containment facilities, Miner. Eng. 22 (2009) 840–848, https://doi.org/10.1016/j.mineng.2009.02.011.

[13] Y. Guney, B. Cetin, A.H. Aydilek, B.F. Tanyu, S. Koparal, Utilization of sepiolite materials as a bottom liner material in solid waste landfills, Waste Manag 34 (2014) 112–124, https://doi.org/10.1016/j.wasman.2013.10.008.

[14] Rijkswaterstaat Bodem+, Guidelines for the Implementation of the Landfill Decree on Soil Protection, (1991) 88. https://www.bodemplus.nl/@132149/richtlijnen-uitvoeringsregeling-stortbesluit/.

[15] E. Commission, The European Green Deal, Brussels, 2019.

[16] Y.L. Li, J.W. Liu, J.Y. Chen, Y.F. Shi, W. Mao, H. Liu, Y. Li, S. He, J.K. Yang, Reuse of dewatered sewage sludge conditioned with skeleton builders as landfill cover material, Int. J. Environ. Sci. Technol. 11 (2014) 233–240, https://doi.org/10.1007/s13762-013-0199-y.

[17] S. Oh, W.S. Shin, Applicability of solidified/stabilized dye sludge char as a landfill cover material, KSCE J. Civ. Eng. 21 (2017) 2573–2583, https://doi.org/10.1007/s12205-017-0064-5.

[18] N.A. Rosli, H.A. Aziz, M.R. Selamat, L.L.P. Lim, A mixture of sewage sludge and red gypsum as an alternative material for temporary landfill cover, J. Environ. Manag. 263 (2020) 110420, https://doi.org/10.1016/J.JENVMAN.2020.110420.

[19] E.H. Kim, J.K. Cho, S. Yim, Digested sewage sludge solidification by converter slag for landfill cover, Chemosphere 59 (2005) 387–395, https://doi.org/10.1016/j.chemosphere.2004.10.038.

[20] M. Liu, H. Lu, Q. Deng, S. Ji, L. Qin, Y. Wan, Shear strength, water permeability and microstructure of modified municipal sludge based on industrial solid waste containing calcium used as landfill cover materials, Waste Manag 145 (2022) 20–28, https://doi.org/10.1016/J.WASMAN.2022.04.031.

[21] M. Barjenbruch, O. Kopplow, Enzymatic, mechanical and thermal pre-treatment of surplus sludge, Adv. Environ. Res. 7 (2003) 715–720, https://doi.org/10.1016/S1093-0191(02)00032-1.

[22] B. Wett, P. Phothilangka, A. Eladawy, Systematic comparison of mechanical and thermal sludge disintegration technologies, Waste Manag 30 (2010) 1057–1062, https://doi.org/10.1016/j.wasman.2009.12.011.

[23] X. Gao, Q.L. Yu, A. Lazaro, H.J.H. Brouwers, Investigation on a green olivine nano-silica source based activator in alkali activated slag-fly ash blends: reaction kinetics, gel structure and carbon footprint, Cem. Concr. Res. 100 (2017) 129–139, https://doi.org/10.1016/j.cemconres.2017.06.007.

[24] M. Wiśniewska, W. Stępniewski, 2006. The influence of lime, water-glass and clay addition on sealing properties of waste rock from Bogdanka, in: Environ. Eng. Proc. 2nd Natl. Congr. Environ. Eng. 4–8 Sept. 2005, CRC Press: p. 271.

[25] M. Tramontin, L. Simão, O. Rubem, K. Montedo, F. Raupp, A. Pedro, N. De Oliveira, Aluminum anodizing waste and its uses: an overview of potential applications and market opportunities, Waste Manag 84 (2019) 286–301, https://doi.org/10.1016/j.wasman.2018.12.003.

[26] M.J. Ribeiro, J.A. Labrincha, Properties of sintered mullite and cordierite pressed bodies manufactured using Al-rich anodising sludge 34 (2008) 593–597, https://doi.org/10.1016/j.ceramint.2006.12.005.

[27] C.A. Grattoni, X.D. Jing, R.W. Zimmerman, Disproportionate Permeability Reduction when a Silicate Gel is Formed In-Situ to Control Water Production, SPE Lat. Am. Caribb. Pet. Eng. Conf. (2001) SPE-69534-MS. https://doi.org/10.2118/69534-MS.

[28] D..Boels, J..Bril, E..Hummelink, O..Boersma, Durability of Hydrostab; a field investigation and prognosis, Wageningen, 2005. ⟨https://edepot.wur.nl/25573⟩.

[29] S. Brunauer, P.H. Emmett, E. Teller, Adsorption of gases in multimolecular Layers, J. Am. Chem. Soc. 60 (1938) 309–319, https://doi.org/10.1021/ja01269a023.

[30] S. Barzgar, M. Tarik, C. Ludwig, B. Lothenbach, The effect of equilibration time on Al uptake in C-S-H, Cem. Concr. Res. 144 (2021) 106438, https://doi.org/10.1016/j.cemconres.2021.106438.

[31] Z. Jinhong, L. Qimei, Z. Xiaorong, The hydrochar characters of municipal sewage sludge under different hydrothermal temperatures and durations, J. Integr. Agric. 13 (2014) 471–482, https://doi.org/10.1016/S2095-3119(13)60702-9.

[32] M. Horgnies, J.J. Chen, C. Bouillon, Overview about the use of fourier transform infrared spectroscopy to study cementitious materials, WIT Trans. Eng. Sci. 77 (2013) 251–262, https://doi.org/10.2495/MC130221.

[33] P. Thipkhunthod, V. Meeyoo, P. Rangsunvigit, T. Rirksomboon, Describing sewage sludge pyrolysis kinetics by a combination of biomass fractions decomposition, J. Anal. Appl. Pyrolysis 79 (2007) 78–85, https://doi.org/10.1016/j.jaap.2006.10.005.

[34] J. De Oliveira Silva, G.R. Filho, C. Da Silva Meireles, S.D. Ribeiro, J.G. Vieira, C. V. Da Silva, D.A. Cerqueira, Thermal analysis and FTIR studies of sewage sludge produced in treatment plants. the case of sludge in the city of Uberlândia-MG, Brazil, Thermochim. Acta 528 (2012) 72–75, https://doi.org/10.1016/j.tca.2011.11.010.

[35] L. Tourneret, F. Berger, C. Mavon, A. Chambaudet, Calcium sulphate formation during the heat-up period: some essential parameters, Appl. Clay Sci. 14 (1999) 299–317, https://doi.org/10.1016/S0169-1317(99)00005-8.

[36] M.A. Tantawy, M.R. Shatat, M.A. Taher, M.A. Taher, M. Abd-El-Hamed, Low temperature synthesis of belite cement based on silica fume and lime, Int. Sch. Res. Not. 2014 (2014) 10, https://doi.org/10.1155/2014/873215.

[37] T. Sun, Q. Zhuo, Y. Chen, Z. Wu, Synthesis of boehmite and its effect on flame retardancy of epoxy resin, High. Perform. Polym. 27 (2015) 100–104, https://doi.org/10.1177/0954008314540312.

[38] M. Li, B. Xiao, X. Wang, J. Liu, Consequences of sludge composition on combustion performance derived from thermogravimetry analysis, Waste Manag 35 (2015) 141–147, https://doi.org/10.1016/j.wasman.2014.10.004.
[39] P. Gahlot, G. Balasundaram, V. Kumar, A.E. Atabani, D. Juchelkov, Principles and potential of thermal hydrolysis of sewage sludge to enhance anaerobic digestion, 214 2022. https://doi.org/10.1016/j.envres.2022.113856.
[40] C. Rodriguez-Navarro, E. Ruiz-Agudo, A. Luque, A.B. Rodriguez-Navarro, M. Ortega-Huertas, Thermal decomposition of calcite: mechanisms of formation and textural evolution of CaO nanocrystals, Am. Mineral. 94 (2009) 578–593, https://doi.org/10.2138/am.2009.3021.
[41] M. Park, S. Lee, H. Kim, I. Park, J. Choy, Tailoring porosity of colloidal boehmite sol by controlling crystallite size, Bull. Korean Chem. Soc. 33 (2012) 1962–1966, https://doi.org/10.5012/bkcs.2012.33.6.1962.
[42] K. Miao, Z. Wang, R. He, L. Jin, Z. Song, R. Yu, Z. Lu, D. Li, Effects of boehmite on the calcination shrinkage and mechanical properties of gypsum-bonded molds, Adv. Eng. Mater. 24 (2022), https://doi.org/10.1002/adem.202100683.
[43] H.B. Nagaraj, B. Reesha, M.V. Sravan, M.R. Suresh, Correlation of compaction characteristics of natural soils with modified plastic limit, Transp. Geotech. 2 (2015) 65–77, https://doi.org/10.1016/j.trgeo.2014.09.002.
[44] Rijkswaterstaat, Guidelines implementing the landfill decision on soil protection, 1991. 88. ⟨https://www.bodemplus.nl/@132149/richtlijnen-uitvoeringsregeling-stortbesluit/⟩.
[45] H. Zhang, B. Yang, G. Zhang, X. Zhang, Sewage sludge as barrier material for heavy metals in waste landfill, Arch. Environ. Prot. 42 (2016) 52–58, https://doi.org/10.1515/aep-2016-0020.
[46] D.A. Rubinos, G. Spagnoli, Utilization of waste products as alternative landfill liner and cover materials–a critical review, Crit. Rev. Environ. Sci. Technol. 48 (2018) 376–438, https://doi.org/10.1080/10643389.2018.1461495.
[47] J.Q. Chen, T.R. Liu, M.M. Sun, Y.Z. Zhao, H.H. Ge, Inhibition of poly (Ethylenediaminetetraacetic acid-diethanolamine) on deposition of calcium sulfate crystal in simulated industrial water, Crystals 10 (2020) 1–15, https://doi.org/10.3390/cryst10060544.
[48] A.M.B. Silva, D.O. Junot, L.V.E. Caldas, D.N. Souza, Structural, optical and dosimetric characterization of CaSO4:Tb, CaSO4:Tb, Ag and CaSO4:Tb,Ag(NP), J. Lumin. 224 (2020), https://doi.org/10.1016/j.jlumin.2020.117286.
[49] I. García-Lodeiro, A. Fernández-Jiménez, M.T. Blanco, A. Palomo, FTIR study of the sol-gel synthesis of cementitious gels: C-S-H and N-A-S-H, J. Sol. Gel Sci. Technol. 45 (2008) 63–72, https://doi.org/10.1007/s10971-007-1643-6.
[50] Y. Pan, S. He, X. Cheng, Z. Li, C. Li, Y. Huang, L. Gong, A fast synthesis of silica aerogel powders-based on water glass via ambient drying, J. Sol. Gel Sci. Technol. 82 (2017) 594–601, https://doi.org/10.1007/s10971-017-4312-4.
[51] F. Paulik, J. Paulik, M. Arnold, Thermal decomposition of gypsum, Thermochim. Acta 200 (1992) 195–204, https://doi.org/10.1016/0040-6031(92)85115-C.
[52] K. Scrivener, R. Snellings, B. Lothenbach, A practical guide to microstructural analysis of cementitious materials, Crc Press, Boca Raton, FL, USA, 2016, https://doi.org/10.1201/b19074.
[53] Y. Ma, J. Hu, G. Ye, The pore structure and permeability of alkali activated fly ash, Fuel 104 (2013) 771–780, https://doi.org/10.1016/j.fuel.2012.05.034.
[54] A.A. Amadi, A.O. Eberemu, Potential application of lateritic soil stabilized with cement kiln dust (CKD) as liner in waste containment structures, Geotech. Geol. Eng. 31 (2013) 1221–1230, https://doi.org/10.1007/s10706-013-9645-3.
[55] J. Sung, H. Song, G. Yim, S. Woo, J. Kim, An engineered cover system for mine tailings using a hardpan layer: a solidification / stabilization method for layer and field performance evaluation, J. Hazard. Mater. 197 (2011) 153–160, https://doi.org/10.1016/j.jhazmat.2011.09.069.
[56] S.A. Stronach, F.P. Glasser, Modelling the impact of abundant geochemical components on phase stability and solubility of the CaO-SiO2 -H2O system at 25 °C: Na+, K +, SO42-, Cl- and CO32-, Adv. Cem. Res. 9 (1997) 167–181, https://doi.org/10.1680/adcr.1997.9.36.167.
[57] H. Song, S. Kwon, 2007. Permeability characteristics of carbonated concrete considering capillary pore structure, 37. 909–915. https://doi.org/10.1016/j.cemconres.2007.03.011.
[58] R.W. Zuhl, Z. Amjad, 2013. Solution Chemistry Impact on Silica Polymerization by Inhibitors, in: Miner. Scales Biol. Ind. Syst., 2013: p. 173. https://doi.org/10.1201/b15606–13.
[59] P. Singh, A. Borthakur, R. Singh, R. Bhadouria, A critical review on the research trends and emerging technologies for arsenic decontamination from water, Groundw. Sustain. Dev. 14 (2021) 100607, https://doi.org/10.1016/j.gsd.2021.100607.
[60] C.H. Weng, C.P. Huang, H.E. Allen, A.H. Cheng, P.F. Sanders, Chromium leaching behavior in soil derived from chromite ore processing waste, Sci. Total Environ. 154 (1994) 71–86, https://doi.org/10.1016/0048-9697(94)90615-7.
[61] C.E. Halim, S.A. Short, J.A. Scott, R. Amal, G. Low, Modelling the leaching of Pb, Cd, As, and Cr from cementitious waste using PHREEQC, J. Hazard. Mater. 125 (2005) 45–61, https://doi.org/10.1016/j.jhazmat.2005.05.046.
[62] L.A. Mendes, L. Felipe, P. Bucater, M.D. Landgraf, M. Olímpia, O. Rezende, Role of organic matter in the adsorption / desorption of Cr, Cu and Pb in competitive systems in two different soils, Open Access Libr. J. 1 (2014) 1–5, https://doi.org/10.4236/oalib.1101022.
[63] J.J.G. Costa, M.J. Reigosa, J.M. Matías, E.F. Covelo, Soil Cd, Cr, Cu, Ni, Pb and Zn sorption and retention models using SVM: Variable selection and competitive model, Sci. Total Environ. 593– 594 (2017) 508–522, https://doi.org/10.1016/j.scitotenv.2017.03.195.
[64] Rijkswaterstaat, Landfills in the Netherlands, 2022. ⟨https://www.bodemplus.nl/onderwerpen/bodem-ondergrond/verwerking-grond/stortplaatsen/stortplaatsen/⟩ (accessed March 29, 2022).